Output-Error Methods in Structural Modal Identification

Mehran Pourgholi[1*], Mehdi Koohdaragh[2]
1- Department of Civil Engineering, Sarab Branch, Islamic Azad University, Sarab, Iran.
2- Department of Civil Engineering, Malekan Branch, Islamic Azad University, Malekan, Iran.
*pourgholi@iausa.ac.ir

ABSTRACT

Stochastic subspace identification (SSI) is a process that linearizes the identification problem by utilizing singular value decomposition (SVD) and QR factorization. This technique enables the extraction of system matrices through linear least squares. However, the estimated systems in these methods are affected by the user-defined dimensions of the data space (Hankel matrix). Also, SSI does not explicitly minimize a cost function for estimating system matrices, making statistical analysis difficult. To enhance the accuracy of modal specifications obtained from SSI, especially the damping ratios, this research suggests using output-error methods (OEM). During OEM, the process involves iteratively adjusting the model parameters to match the outputs of the simulated model with those of the observed system. The following steps are taken to enhance the OEM for extracting structural properties: Firstly, the initial term is derived using the SSI to reduce the number of optimization iterations. Secondly, by using the Gauss-Newton approach, the nonlinearity of the objective function is reduced by treating the second-order derivatives as a linear system. Finally, Gradient project minimization is utilized in SSI to ensure the injectivity of estimated systems. The OEM was validated by analyzing the response of a 3-DOF excited by white noise with an SNR of 1 db. Then, the model was then applied to seismic observations of Pacoima Dam during the 2001 San Fernando and 2008 Chino Hills earthquakes. The two main modes of the structure were extracted, and they had the least error compared to the developed finite element models.

Key words: System Identification, Output-Error method, Gauss-Newton, gradient projection, Pacoima Dam.

1.INTRODUCTION

Quantifying the dynamic characteristics of structures (frequency, damping ratio, and mode shapes) is an essential tool for studying their dynamic response against excitation, such as earthquakes, wind, and explosions [1]. This can be achieved through ambient and forced vibration testing. In flexible structures such as dams, bridges, and buildings forced vibration tests (FVT) are considered more reliable because they involve controlled vibrations that enhance the dynamic response of the structure. This results in better noise source overlap and increases the accuracy of the extracted modal characteristics. Additionally, these tests provide valuable information about the mass and rigidity of the structure, which can be used to update the finite element model quickly[2, 3].

One of the most popular methods for analyzing the results of dynamic vibration tests is the stochastic subspace identification (SSI) method. These methods modulate the vibrating structure in the state space as a Linear Time-Invariant (LTI) system [4, 5]. These methods are based on arranging measured inputs and outputs in the Hankel matrix [6]. By solving the linear least squares (LS) problem, the modal properties may be determined utilizing essential linear algebraic techniques such as rank-querying (RQ) and singular value decomposition (SVD). Bypassing the nonlinear

modes is one of the main reasons for the popularity of these methods [7-9]. Various algorithms have been presented for these methods based on how to deal with input and output noises, such as PI-MOESP for colored noises and PO-MOESP for white noises approach [10]. Other algorithms include N4SID, based on the least squares [11]and SI-ORT, based on the canonical correlation analysis [12, 13].

The output-error method (OEM) is another approach to analyzing FVT, the standard methodology for estimating aircraft parameters [14, 15]. These approaches' foundation is the iterative matching of the simulated model response with the measured response [16-18].The approach assumes that the uncertainties caused by the noises operating on the system are additively perturbed at the output [19-22]. It consists of four phases: The first phase entails parameterizing the model or choosing the parameters to estimate in the model. In the second step, the estimate of model parameters is formulated as an optimization problem. Step three is selecting a numerical method to solve the optimization issue iteratively. The last stage is a covariance matrix-based assessment of the correctness of the derived estimations. White noise with zero means is assumed as an additive error throughout these four stages.

As previously stated, this approach is used chiefly for aeronautical themes [23, 24]; nevertheless, it has lately been utilized to determine robot features [25]. This technique has recently been applied to deterministic dynamics in industrial processes, including temporal delays and unknown load disturbances [26]. However, this method's potential has yet to be explored in structural problems. This study plans to employ OEM, which has never been used in system identification procedures through an ambient vibration test, to extract structural modal features. In the OEM approach, parameter estimation is carried out using a nonlinear optimization methodology (Gauss-Newton method). Consequently, the method is more computationally demanding due to its iterative nature. This approach was applied to the modal test of structures as follows:

First, the starting statement is collected from the SSI to limit the number of trials and mistakes and the dependency of the detected modal features on the initial response utilized in the optimization. Second, the objective function's complexity is reduced by considering the second-order derivatives as a linear system to optimize parameters using the Gauss-Newton approach. Finally, due to the non-injectivity of the specified parameterization and similarity transformations of the state-space systems, the objective function is updated outside the same transformations to prevent numerical difficulties in the gradient project minimization process.

The proposed algorithm extracts the modal characteristics of Pacoima Dam using its seismic data after validation with a numerical model of a 3DOF analytical system with closely spaced modes under different noise intensities.

2.Output-Error Method

In ambient vibration testing, data is collected at certain intervals, such as kt. By using the following set of discrete time equations in the state space, the dynamic behavior of the desired structure can be described:

$$x(k+1) = \mathbf{A}x(k) + \mathbf{B}u(k) + \omega_k \quad (1)$$

$$y(k) = \mathbf{C}x(k) + \mathbf{D}u(k) + \vartheta_k \quad (2)$$

where $x \in \mathbb{R}^{2.n\times 1}$ is a discrete stochastic vector at time instant k, $y \in \mathbb{R}^{m\times 1}$ denotes the sampled outputs vector at the $k-th$ time step, $u(k) \in \mathbb{R}^{s\times 1}$ is the input or control vector, $\mathbf{A} \in \mathbb{R}^{2.n\times 2.n}$ sows the discrete-time state matrix and $\mathbf{C} \in \mathbb{R}^{m\times n}$ represents the output matrix, m is the number of measurement points or sensors, $\omega_k \in \mathbb{R}^{2.n\times 1}$ and $\vartheta_k \in \mathbb{R}^{m\times 1}$ are measurement and computation noises, respectively [27]. It is important to note that the signal-generating LTI system can describe the vibrating structure's dynamic response (Eq. 2) as:

$$y(k) = G(q)u(k) + v_k \tag{3}$$

Where *k=1, 2,..., s* is the total quantity of measured data, $G(q)$ is the system's deterministic component, and $v_k \in \mathbb{R}^{m\times 1}$ stands for measurement noise that is statistically independent from the inputs ($u \in \mathbb{R}^{s\times 1}$).

The objective of modelling in the OEM (Fig.1) is to find a collection of system matrices (**A**, **B**, **C**, **D**) such that the output $\hat{y}(k)$ approximates the system's output $y(k)$ (Eq.3). One frequent strategy for solving this issue is estimating a vector of parameters (Eq.4) based on the assumption that the system's matrix entries depend on these parameters.

$$\theta = \begin{bmatrix} \theta_{AC} \\ \theta_{BD} \end{bmatrix} = \begin{bmatrix} \begin{bmatrix} vec(A) \\ vec(C) \end{bmatrix} \\ \begin{bmatrix} \hat{x}(0) \\ vec(B) \\ vec(D) \end{bmatrix} \end{bmatrix} \tag{4}$$

Where $vec(.)$ represents the vector operator, θ_{AC} is the set of parameters required for the system outputs, and θ_{BD} is the parameter vector of the system inputs[28]. According to the Eqs.1a and 2b, the estimated system may be parameterized as follows using the parameter vector θ as follows:

$$\hat{x}(k+1,\theta) = \mathbf{A}(\theta)\hat{x}(k,\theta) + \mathbf{B}(\theta)u(k) \tag{5.a}$$

$$\hat{y}(k,\theta) = \mathbf{C}(\theta)\hat{x}(k,\theta) + \mathbf{D}(\theta)u(k) \tag{5.b}$$

To estimate the state-space model, the following quadratic cost function is considered[29-32]:

$$\mathbf{J}_N(\theta) = \frac{1}{N}\sum_{k=0}^{N-1} y(k) - \hat{y}(k,\theta)_2^2 = \frac{1}{N}\begin{bmatrix} y(k)-\hat{y}(0,\theta) \\ y(k)-\hat{y}(1,\theta) \\ . \\ . \\ . \\ \epsilon(N-1,\theta) \end{bmatrix}^T \begin{bmatrix} y(k)-\hat{y}(0,\theta) \\ y(k)-\hat{y}(1,\theta) \\ . \\ . \\ . \\ \epsilon(N-1,\theta) \end{bmatrix} = \frac{1}{N}E_N^T(\theta)E_N(\theta) \tag{6}$$

where $y(k)$ is the measured output signal, $\hat{y}(k,\theta)$ is the output signal of the model and $E_N(\theta)$ is the prediction error vector.

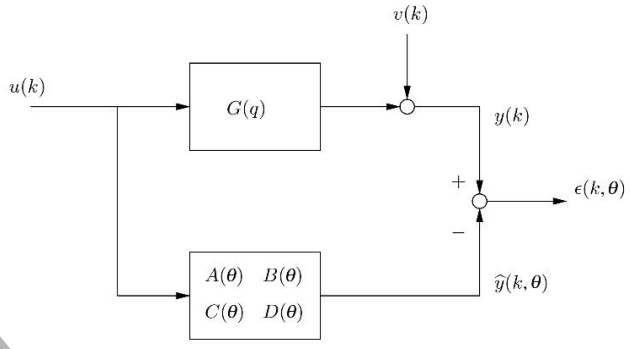

Fig.1 The output-error model-estimation method

The cost function $\mathbf{J}_N(\theta)$ is a scalar function that depends on the parameter vector θ in the parameter space Ω. The problem of its optimization by considering the constraints can be expressed as follows:

$$\underset{\theta \in \Omega \subset R^p}{\text{minimize}} \ \mathbf{J}_N(\theta) = \frac{1}{N} E_N^T(\theta) E_N(\theta) \tag{7.a}$$

$$\text{Subject to} \begin{cases} \hat{x}(0,\theta) = \hat{x}(0) \\ \hat{x}(k+1,\theta) = \mathbf{A}(\theta)\hat{x}(k,\theta) + \mathbf{B}(\theta)u(k) \\ \hat{y}(k,\theta) = \mathbf{C}(\theta)\hat{x}(k,\theta) + \mathbf{D}(\theta)u(k) \end{cases} \tag{7.b}$$

Specifically, the following Taylor series expansion in $E_N(\theta)$ about i is utilized to provide a numerical solution to the parameter-optimization problem[21]:

$$\begin{aligned} \underset{\delta\theta^{(i)}}{\min} \frac{1}{N}\left(\mathbf{J}_N\left(\theta^{(i)} + \delta\theta^{(i)}\right) = \frac{1}{N} E_N\left(\theta^{(i)} + \delta\theta\right)_2^2 \right) \\ \approx \underset{\delta\theta^{(i)}}{\min} \frac{1}{N} E_N\left(\theta^{(i)} + \frac{\partial E_N(\theta)}{\partial \theta^T} \delta\theta^i \right)_2^2 \end{aligned} \tag{8}$$

By defining $\delta\theta^i = \theta^{(i+1)} - \theta^i$ and marking $\boldsymbol{\psi}_N(\theta) = \dfrac{\partial E_N(\theta)}{\partial \theta^T}$, the preceding linear least squares problem is solved in the way presented:

$$\begin{aligned} \theta^{(i+1)} &= \theta^i - (\boldsymbol{\psi}_N\left(\theta^{(i)}\right)^T \boldsymbol{\psi}_N\left(\theta^{(i)}\right))^{-1} \boldsymbol{\psi}_N\left(\theta^{(i)}\right)^T E_N\left(\theta^{(i)}\right) \\ &= \theta^i - \left(\mathbf{H}_N\left(\theta^{(i)}\right)\right)^{-1} \mathbf{J}_N^{'}\left(\theta^{(i)}\right) \end{aligned} \tag{9}$$

where $\mathbf{H}_N\left(\theta^{(i)}\right)$ is the Hessian matrix and $\mathbf{J}_N^{'}\left(\theta^{(i)}\right)$ is the Jacobian of objective function.

Eq.9 shows that $E_N(\theta)$ and $\boldsymbol{\psi}_N(\theta)$ must be determined for each iteration. From the set of Eq.1, we can derive the matrix $E_N(\theta)$, but to compute $\boldsymbol{\psi}_N(\theta)$, we need to have:

$$\psi_N(\theta)=\begin{bmatrix}\frac{\partial \mathrm{E}(0,\theta)}{\partial\theta^T}\\ \frac{\partial \mathrm{E}(1,\theta)}{\partial\theta^T}\\ \cdot\\ \cdot\\ \cdot\\ \frac{\partial \mathrm{E}(N-1,\theta)}{\partial\theta^T}\end{bmatrix}=-\begin{bmatrix}\frac{\partial \hat{y}(0,\theta)}{\partial\theta^T}\\ \frac{\partial \hat{y}(1,\theta)}{\partial\theta^T}\\ \cdot\\ \cdot\\ \cdot\\ \frac{\partial \hat{y}(N-1,\theta)}{\partial\theta^T}\end{bmatrix} \tag{10}$$

where

$$\frac{\partial \hat{y}(k,\theta)}{\partial\theta^T}=\begin{bmatrix}\frac{\partial \hat{y}(k,\theta)}{\partial\theta(1)} & \frac{\partial \hat{y}(k,\theta)}{\partial\theta(2)} & \cdots & \frac{\partial \hat{y}(k,\theta)}{\partial\theta(p)}\end{bmatrix} \tag{11}$$

where $\theta(i)$ represents the *i*th entry in the vector θ. It is straightforward to see that for every parameter $\theta(i)$ we have

$$X_i(k+1,\theta)=\mathbf{A}(\theta)X_i(k,\theta)+\frac{\partial \mathbf{A}(\theta)}{\partial\theta(i)}\hat{x}(k,\theta)+\frac{\partial \mathrm{B}(\theta)}{\partial\theta(i)}u(k) \tag{12}$$

$$\frac{\partial \hat{y}(k,\theta)}{\partial\theta(i)}=\mathbf{C}(\theta)X_i(k,\theta)+\frac{\partial \mathbf{C}(\theta)}{\partial\theta(i)}\hat{x}(k,\theta)+\frac{\partial \mathbf{D}(\theta)}{\partial\theta(i)}u(k) \tag{13}$$

where $X_i(k,\theta)=\frac{\partial \hat{x}(k,\theta)}{\partial\theta(i)}$.

The two preceding equations demonstrate that the derivative of $\partial\hat{y}(k,\theta)$ to $\theta(i)$ may be determined by simulating a linear system with state $X_i(k,\theta)$ and inputs $\hat{x}(k,\theta)$ and $u(k)$.

Note that the matrices $\frac{\partial \mathbf{A}(\theta)}{\partial\theta(i)}, \frac{\partial \mathbf{B}(\theta)}{\partial\theta(i)}, \frac{\partial \mathbf{C}(\theta)}{\partial\theta(i)}$, and $\frac{\partial \mathbf{D}(\theta)}{\partial\theta(i)}$ are fixed and solely rely on the specific parameterization used to describe the system. Our investigation leads us to the conclusion that determining $\psi_N(\theta)$ is equivalent to running a linear system model for each component of the θ parameter vector. The simulation of p+1 linear systems is required to calculate $\psi_N(\theta)$ and $E_N(\theta)$ if θ has p parameters.

System matrices in the state space are non-injective so a singular Hessian matrix can be generated. Consequently, multiple combinations of parameters provide the same value for the cost function $\mathbf{J}_N(\theta)$. Hence the θ that minimizes $\mathbf{J}_N(\theta)$ is no longer required to be unique. Here, we investigate an arbitrary system with matrices $(\bar{\mathbf{A}},\bar{\mathbf{B}},\bar{\mathbf{C}},\bar{\mathbf{D}})$ using the transformation matrix $\mathbf{T}\in\mathbb{R}^{n\times n}$ from the system $(\mathbf{A},\mathbf{B},\mathbf{C},\mathbf{D})$:

$$\begin{bmatrix} \bar{\mathbf{A}} & \bar{\mathbf{B}} \\ \bar{\mathbf{C}} & \bar{\mathbf{D}} \end{bmatrix} = \begin{bmatrix} \mathbf{T}^{-1}\mathbf{A}\mathbf{T} & \mathbf{T}^{-1}\mathbf{B} \\ \mathbf{C}\mathbf{T} & \mathbf{D} \end{bmatrix} \tag{14}$$

A manifold is obtained in the parametric space by applying all the non-singular $\mathbf{T} \in \mathbb{R}^{n \times n}$ in the above relation. In order to minimize the objective function, one should avoid moving along it because the objective function is fixed on it. A perturbation equal to $\Delta\mathbf{T}$ is applied to the identity matrix $\mathbf{I}_N$ to determine the tangent plane on this manifold[33, 34].

$$\mathbf{T} = \mathrm{I}_n + \Delta\mathbf{T} \tag{15}$$

The following expression is a first-order approximation of similarly comparable systems:

$$\begin{bmatrix} \bar{\mathbf{A}} & \bar{\mathbf{B}} \\ \bar{\mathbf{C}} & \bar{\mathbf{D}} \end{bmatrix} = \begin{bmatrix} \mathbf{A} & \mathbf{B} \\ \mathbf{C} & \mathbf{D} \end{bmatrix} + \begin{bmatrix} \mathbf{A}\Delta\mathbf{T} - \Delta\mathbf{T}\mathbf{A} & -\Delta\mathbf{T}\mathbf{B} \\ \mathbf{C}\Delta\mathbf{T} & 0 \end{bmatrix} \tag{16}$$

Based on the property of the vector operator (Eq.17), we have the following:

$$vec(\mathbf{XYZ}) = (\mathbf{Z} \otimes \mathbf{X})vec(\mathbf{Y}) \tag{17}$$

$$\bar{\theta} = \theta + \begin{bmatrix} \mathrm{I}_n \otimes \mathbf{A} - \mathbf{A}^T \otimes \mathbf{I}_n \\ -\mathbf{B}^T \otimes \mathbf{I}_n \\ \mathbf{I}_n \otimes \mathbf{C} \\ 0 \end{bmatrix} vec(\Delta\mathrm{T}) = \theta + \mathbf{Q}(\theta)vec(\Delta\mathbf{T}) \tag{18}$$

where θ and $\bar{\theta}$ are vectors of parameters derived from the original and similar systems, and $\otimes$ is the Boolean product operator. Eq.18 demonstrates that the columns of the matrix $\mathbf{Q}(\theta)$ traverse the tangent plane at point θ on the manifold of similar systems. SVD decomposition is used to evaluate the perpendicular component along the tangent plane:

$$\mathbf{Q}(\theta) = \begin{bmatrix} \mathbf{U}(\theta) & \mathbf{U}_\perp(\theta) \end{bmatrix} \begin{bmatrix} \mathbf{\Sigma}(\theta) & 0 \\ 0 & 0 \end{bmatrix} \begin{bmatrix} V_1(\theta)^T \\ \mathbf{V}_2(\theta)^T \end{bmatrix} \tag{19}$$

where $\mathbf{\Sigma}(\theta) > 0$ *and* $\mathbf{U}_\perp(\theta) \in \mathbb{R}^{p \times p-r}$ *,with* $p = n^2 + n(l+m) + lm$ *and* $r = rank\left(\mathbf{Q}(\theta)\right)$.

The columns of the matrix $\mathbf{U}(\theta)$ and $\mathbf{U}_\perp(\theta)$ form a basis for the column space and the orthogonal complement of the column space of $\mathbf{Q}(\theta)$, respectively. The parameter vector θ may be broken down into its components using the matrices $u(\theta)$ and $\mathbf{U}_\perp(\theta)$:

$$\theta = \overbrace{\mathbf{U}(\theta)\mathbf{U}(\theta)^T}^{\mathrm{Q}(\theta)}\theta + \overbrace{\mathbf{U}_\perp(\theta)\mathbf{U}_\perp(\theta)^T}^{\mathrm{Q}_\perp(\theta)}\theta \tag{20}$$

Because the second part is connected to the directions that affect the cost function's value, the effective direction update of Eq. 18 is adjusted as follows.

$$\theta = \overbrace{\mathbf{U}(\theta)\mathbf{U}(\theta)^T}^{Q(\theta)}\theta + \overbrace{\mathbf{U}_\perp(\theta)\mathbf{U}_\perp(\theta)^T}^{Q_\perp(\theta)}\theta \tag{21}$$

Fig. 2 shows a flowchart depicting the OEM procedure.

3. Numerical validation for OEM method

This section provides a comprehensive evaluation of OEM's performance regarding the accuracy and reliability of its estimates for forced vibration. The evaluation is based on a modal analysis of a system with two closely spaced and strong modes (Fig.3), where the distribution of mass and stiffness is irregular. The proposed method's efficiency is tested in varying noise levels with prescribed signal-to-noise ratios (SNR) of 1%, 5%, and 15%. The structural characteristics of the mentioned systems include mass and stiffness matrix as follows:

$$\mathbf{k} = k\begin{bmatrix} 10 & -1 & 0 \\ -1 & 4 & -3 \\ 0 & -3 & 3 \end{bmatrix} \qquad \mathbf{M} = m\begin{bmatrix} 4 & 0 & 0 \\ 0 & 3 & 0 \\ 0 & 0 & 2 \end{bmatrix} \tag{22}$$

where m=10 ton and k=1500 KN/m are assumed. Also, Cauchy damping has been adopted for both models. The exact values of modal characteristics for the considered case studies are presented in Table 1.

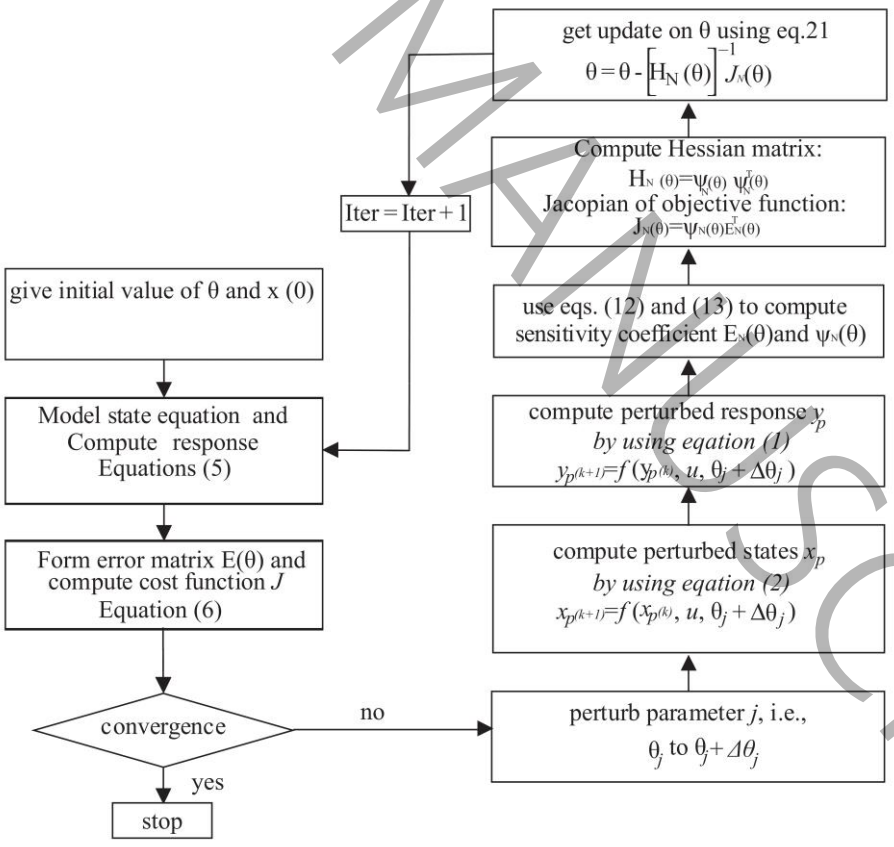

Fig.2 Flowchart of OEM algorithm**.**

The vibration data is created by applying random white noise horizontally at node 1, and the acceleration data is taken as the output. The computed response is affected by sensor noise. The damped response of the system was determined using the fourth-order Runge-Kutta method. The system corresponding to 3-DOF was modeled and analyzed using the Modal analysis technique in the Simulink MATLAB module, as shown in Fig.4. The excitation time was appropriately adjusted for the 30-second recording by the 100 Hz sampling rate, as depicted in Fig.5. For instance, the output record for mass1 is displayed in Fig.6.

Table 1 The modal features of 3-DOF systems determined by the numerical model.

Mode	Frequency (Hz)	Damping (%)
1	0.83	2.00
2	3.00	3.00
3	3.25	4.00

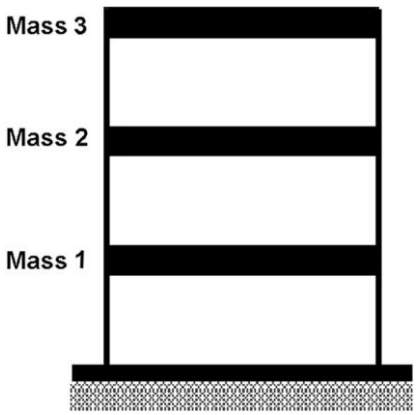

Fig.3 The simulated 3-DOF system

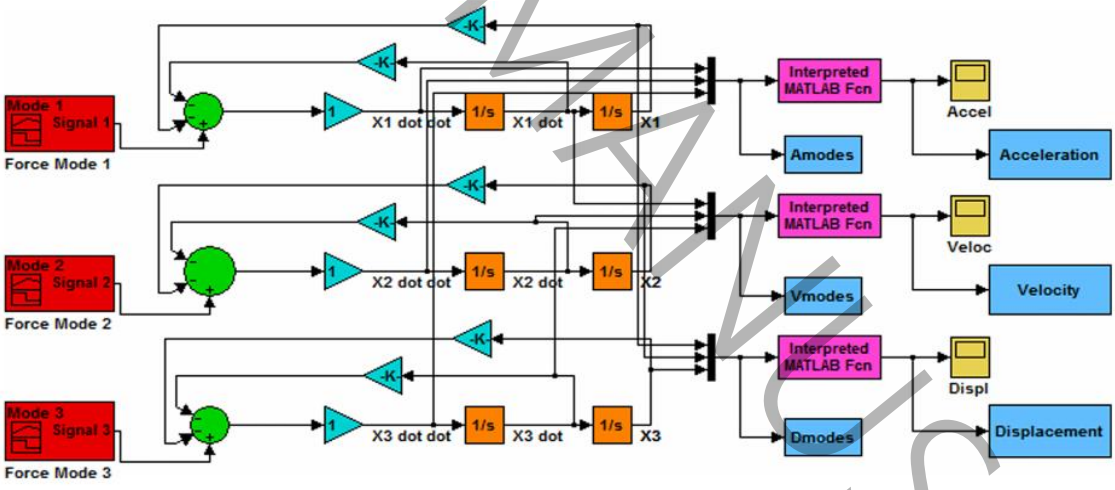

Fig.4. Simulink model of motion differential equations

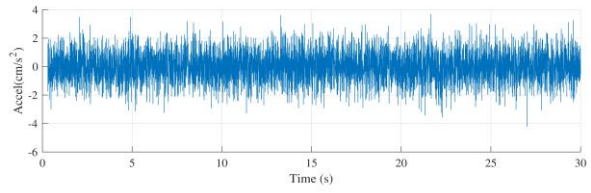

Fig.5 . Random white noise applied in the horizontal direction at mass 1

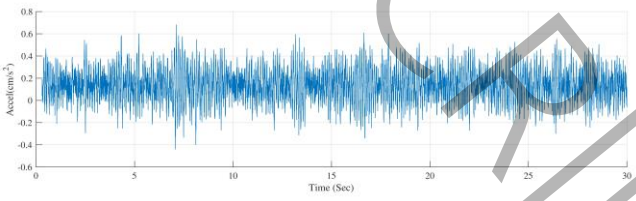

Fig.6. Acceleration records of 3-DOF system at mass 1

4.OEM method in extracting modal characteristics

At first, Modal properties of the structure were detected using the PO-MOESP algorithm to evaluate the effectiveness of the suggested algorithm compared to other identification techniques. To express the estimated error of predicted models in SSI, the variance account for (VAF), an alternative formulation of Eq.6, is employed as follows:

$$VAF = Max\left(0, \left(1 - \frac{\frac{1}{j}\sum_{k=1}^{j}\left(\mathrm{y}_k - \hat{\mathrm{y}}_k\right)^2}{\frac{1}{j}\sum_{k=1}^{j}\left(\mathrm{y}_k\right)^2}\right) \times 100\%\right) \tag{23}$$

where $\mathrm{y}_k \in \mathbb{R}^{m\times j}$ and $\hat{\mathrm{y}}_k \in \mathbb{R}^{m\times j}$ are the measured data and estimated values, respectively. The closer this criterion to 100, the lower the prediction error and the higher the accuracy of the model.

The VAF diagrams of the model is shown in Fig.7.As demonstrated, when SNR decreases, the inaccuracy of the obtained feature grows, bringing the VAF rate from 98% at SNR=5% and SNR=15% to less than 60% at SNR=1dB. One of the known limitations of SSI is that the derived modal properties rely on the Hankel matrix dimensions. Here, we will extract the modal features using the OEM, with the estimated error of the system's response as the objective function. The OEM, defined as the SSI in the state space, will provide the matrices $(\mathbf{A},\mathbf{B},\mathbf{C},\mathbf{D})$. The objective function values have been normalized to 100% based on the maximum value that often occurs in the first step, so the optimization rate can be checked more quickly and readily in both cases. According to Eq.8, the initial point is the most critical limitation a user may decide. In order to make the algorithm's outputs independent of the initial point, more than 30 simulations with initial points with VAFs between 30% and 90% were conducted for each case study. The findings show that adopting predicted models with VAFs between 85 and 90% of the final VAF of the ideal SSI model yields more optimal outcomes, particularly for damping ratios. The explanation is that using phrases with significant estimate errors results in unstable local optimum points. However, the use of starting sentences with very high accuracy in OEM, owing to the optimal character of SSI, yields the same outcomes as SSI. The minimum number of optimization steps is NP=20, and the maximum relative error allowed for optimization stages is 0.1%. The algorithm will terminate if any of these requirements are met before the other. The numerical tests were conducted using MATLAB 2019b on a computer with an Intel Core™ i5-2410 2.30 GHz CPU.

4.1. Extracting modal frequencies and damping ratios of 3-DOF systems with different SNRs

This section analyzes the system identification procedure for the 3-DOF system, which features two closely spaced modes while considering various noise levels. The model's objective function is displayed in Fig. 8 as SNR is altered. As shown in the figure, as the noise level increases (SNR decreases), the objective function converges more slowly for both models. It can be observed that the objective function reaches 90% for SNR=1%, which indicates that model complexity has a significant impact. The VAF diagram in Fig. 7 explains why the optimization process takes longer when the SNR increases. As depicted in the figure, the estimation error also increases with SNR. At an SNR of 15, the estimation error is only 1%, but it surges to over 60% at an SNR of 1%. Fig.9a shows that the first mode

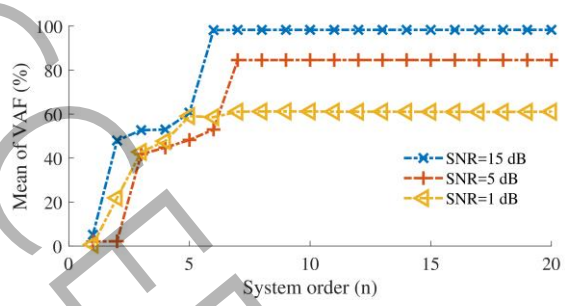

Fig.7. Variance accounting for (VAF) of analytical 3-DoF system obtained from PO-MOESP.

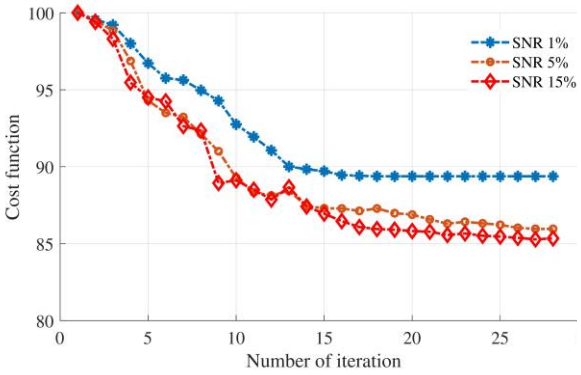

Fig.8. Objective function value evolution process of OEM algorithm.

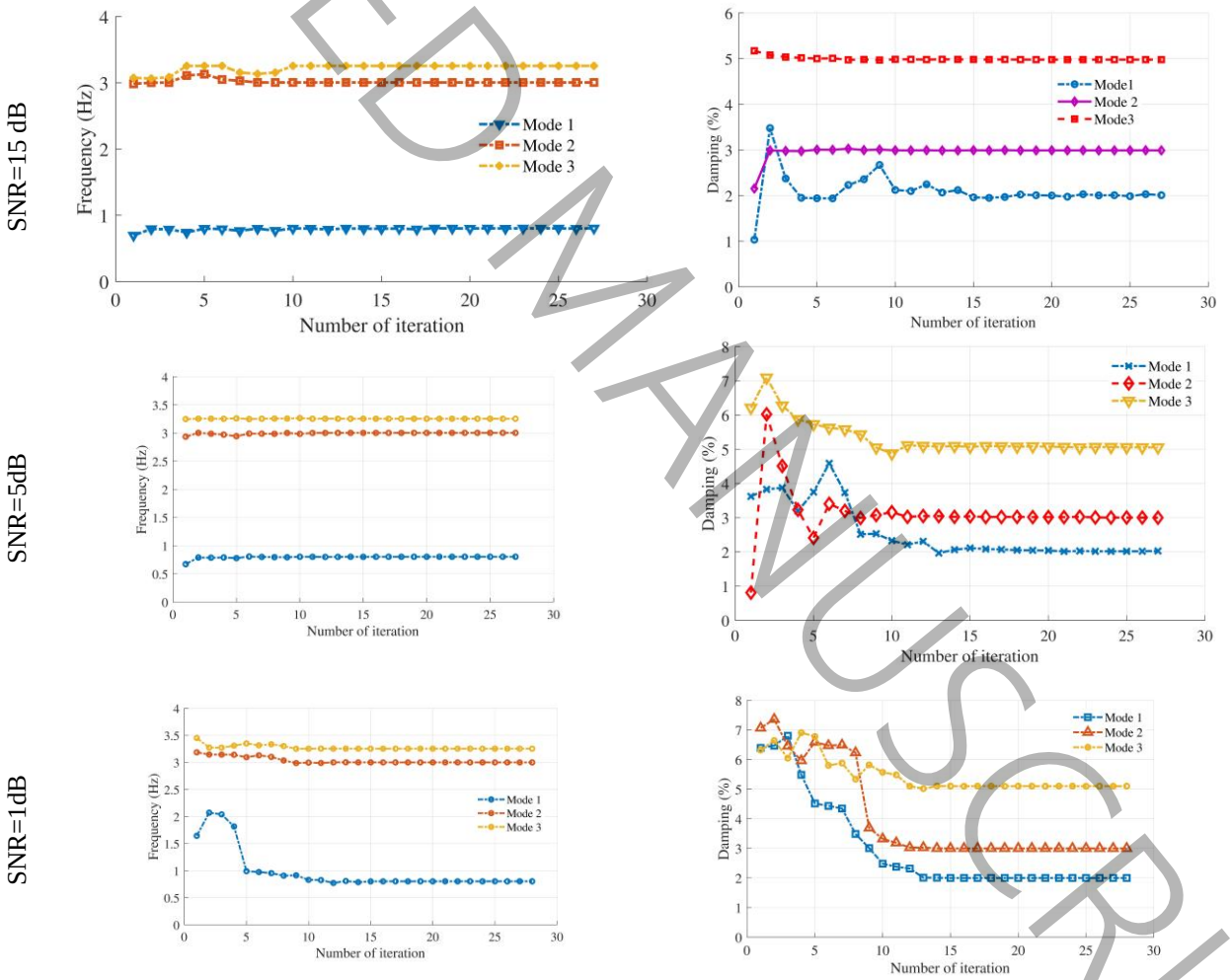

a) Frequency (Hz) b) Damping ratio (%)

Fig.9. System identification process of 3-DOF analytical model for different noise level.

Table 2. Comparison between estimated frequencies and damping ratios of analytical 3-DoF system the reference case (REF). In italic the relative errors in % compared to the FEM case.

SNR (dB)	Mode No.	PO-MOESP		OEM	
		Frequency (Hz)	Damping (%)	Frequency (Hz)	Damping (%)
1	I	0.812 *(1.20)*	2.21 *(10.5)*	0.803 *(0.00)*	2. 02 *(1.00)*
	II	3.17 *(5.70)*	3.178 *(5.93)*	3.00 *(0.00)*	3.07 *(2.33)*
	II	3.48 *(3.00)*	4.9 *(2.00)*	3.20 *(0.00)*	5.05 (*1.00)*
5	I	0.803 *(0.00)*	2.02 *(1.00)*	0.803 *(0.00)*	2.01 *(0.50)*
	II	3.1*(3.33)*	2.99 *(0.00)*	3.00 *(0.00)*	3.01 *(0.33)*
	II	3.24 *(0.03)*	5.04 *(0.80)*	3.26 *(0.00)*	5.05 (*1.00)*
15	I	0.803 *(0.00)*	1.98 *(1.00)*	0.803 *(0.00)*	2.00 *(0.00)*
	II	3.00 *(0.00)*	3.00 *(0.00)*	3.00 *(0.00)*	3.00 *(0.00)*
	II	3.25 *(0.00)*	5.00 *(0.00)*	3.26 *(0.00)*	5.00 *(0.00)*

experienced the most significant frequency changes, and its optimal value was achieved after 11 iterations. The complexity of the model affected the estimation errors of all three-modal damping ratios at 1% and 5% SNRs (Fig.9b). As an SNR of 15% was reached, and the noise intensity decreased, the estimation error for the starting point of the second and third modes was also reduced. However, the modal properties, especially the damping, were successfully optimized for a model with extremely high precision using the proposed algorithm. The optimal values for all three damping ratios are shown in Table 2. This approach reduced the average estimation error for the first and second models in the PO-MOESP from 4.77% and 6.11% to 1%. These findings demonstrate that the proposed algorithm can optimize the modal properties with high accuracy.

4.2. Extracting shape mode of 3-DOF systems with different SNRs

In contrast to damping ratios and modal frequency, form modes are vectors. They cannot be validated using metrics such as variance or relative errors across estimates from different model orders. Thus, other indications, such as the Modal Assurance Criterion (MAC), are often utilized to verify their integrity. The degree of collinearity between two mode shape vectors is represented by the MAC value, which is a real scalar between zero and one. The computation of MAC between two complex-valued mode shapes vectors($\psi \in \mathbb{C}^{m\times 1}$) and estimated at model order n ($\phi \in \mathbb{C}^{m\times 1}$) is as follows[35]:

$$\mathrm{MAC} = \frac{\left|\psi^H \phi\right|^2}{\left(\psi^H \psi\right)\left(\psi^H \psi\right)} = \frac{\psi^H \phi\phi^H \psi}{\psi^H \psi\psi^H \psi} \tag{24}$$

where the symbol ($.^H$) stands for the Hermitian transpose.

The MAC can only provide evidence of continuity; it cannot prove validity or orthogonality. The MAC does not define the existence of identical mistakes in all estimates of modal vectors, whether they are stochastic or biased. Commonly, this kind of possible mistake stems from faulty assumptions. Here, additional criteria derived from the assumption that structures are proportionately dampen are applied to verify the form modes. As a result, the mode shape components lie in a straight line in the complex plane. Modal Complexity Factor (MCF) is one of the modal indicators that aid in defining the complexity of mode shapes[36, 37]. The MCF can be calculated by:

$$\mathrm{MCF}_r = 1 - \frac{\left(S_{xx} - S_{yy}\right)^2 + 4S_{xy}^2}{\left(S_{xx} + S_{yy}\right)^2} \tag{25.a}$$

$$S_{xx} = Re\{\Phi_r\}^T Re\{\Phi_r\} \quad S_{yy} = Im\{\Phi_r\}^T Im\{\Phi_r\} \quad S_{xy} = Re\{\Phi_r\}^T Im\{\Phi_r\} \tag{25.b}$$

where $Re\{\Phi_r\}$ and $Im\{\Phi_r\}$ are the real and imaginary parts of the mode shape vector ($\Phi_r \in \mathbb{C}^{m\times 1}$), respectively. The mode is real if its complexity is close to zero percent, which strongly indicates a natural mode. Complexity levels close to 100% reflect that the mode is complex.

After eigenvalue extraction, the first channel was used as a reference, and all values were scaled accordingly. Mode shapes are only validated for SNR=1dB because, in low-noise models (SNR=5 and 15dB), the eigenvectors are real values (MCF=0%), and the extracted mode shapes likewise show a 100% correlation with the numerical model. The predicted mode shapes, the MAC, and MCF values are shown in Figs.10, and 11, respectively. Fig.11 shows a strong agreement between the mode shapes retrieved by the 3-DOF and the numerical model. In PO-MOESP, the first mode has a MAC value 96.5% (Fig.11a). Nonetheless, the correlation between these two shape modes has grown to 98.9% due to OEM's optimization process. In Fig.11b, the MCF values of the model shows that OEM has improved mode shape complexity such that the first mode has achieved 0.43% from1.45%, respectively. The OEM approach has also decreased the complexity of the second and third-mode shapes by over 80%.

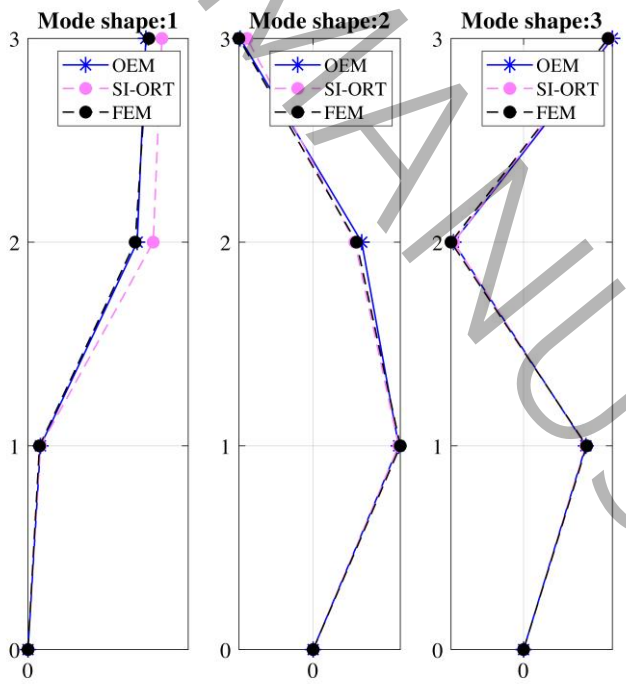

Fig.10: Comparison between mode shapes calculated by FE method and predicted by OEM and PO-MOESP models for SNR=1dB for 3-DOF system with irregular distribution of mass and stiffness.

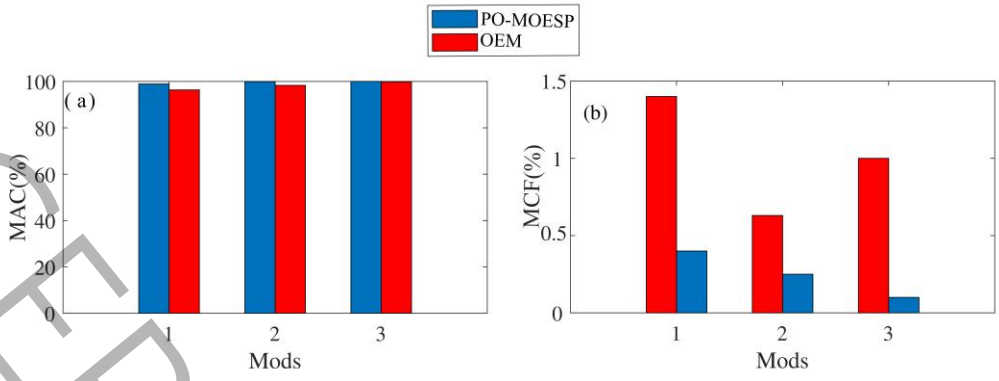

Fig.11: MAC and MCF values between mode shapes calculated by FE method and predicted by OEM and PO-MOESP models for SNR=1Db.

5. System identification of Pacoima dam using earthquake records

The Pacoima Dam (Fig.12) is a concrete arch dam in the San Gabriel Mountains, 5 miles north of San Fernando, near Los Angeles, in Southern California. It was completed in 1982 and stands at a height of 113 meters with a crest length of 180 meters. The dam body varies in thickness from 3 meters at the crest to 30 meters at the bottom and is considered relatively thick for an arch dam. However, it is only designed to withstand static loads and does not consider earthquake forces[38, 39]. Despite experiencing two earthquakes with $A_g > g$ (San Fernando 1971 and Northridge 1994), the structure has also faced several low-intensity earthquakes. As there have been no reports of cracks in the dam body after these low-intensity earthquakes, it is assumed that the dam's behavior during these events is linear. After the 1994 earthquake, the dam was equipped with more than 17 accelerometers in different directions, such as tangential, radial, and vertical, as shown in Fig.12.

The 2001 San Fernando earthquake, which had a magnitude of 4.2 on the Richter scale and was located 7.1 km away from the dam, is one of the best-documented cases of low-intensity earthquakes. Numerous researchers, including Alves, have analyzed these records to determine the dam's modal characteristics. In addition to identifying the

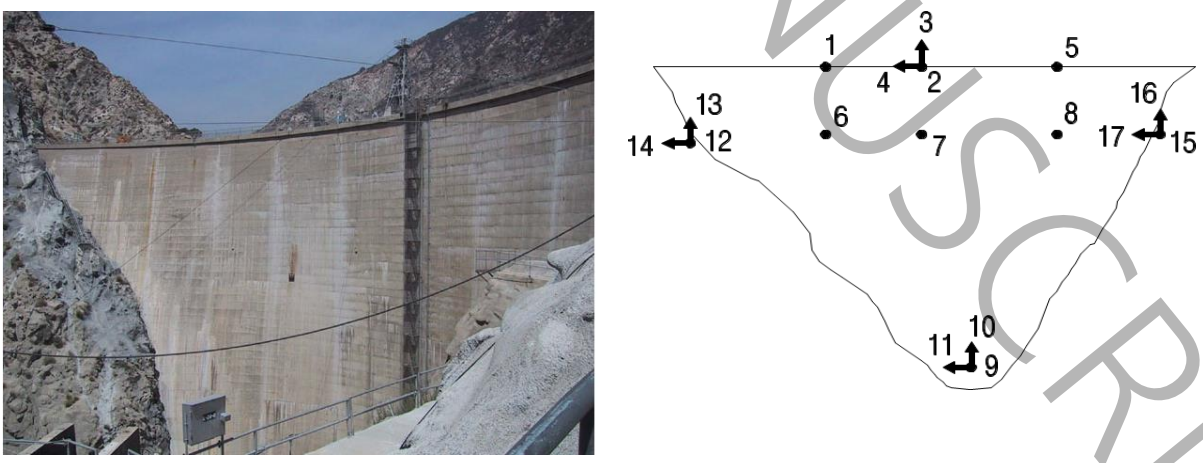

a) View of right abutment **b)** Layout of the 17 acceleration sensors

Fig.12. Pacoima arch dam and the layout of the 17 acceleration sensors[40].

Table3. Modal Characteristics of Pacoima Arch Dam Obtained from San Fernando 2002 and Chino Hills 2008 Earthquake Records.

	mode	San Fernando (2001)		Chino Hills (2008)		FEM	Forced Vibration (2002)	
		Freq. (Hz)	Dam. (%)	Freq. (Hz)	Dam. (%)	Freq. (Hz)	Freq. (Hz)	Dam. (%)
Alves [38-40]	1	4.73-4.83	6.6~7.3	-	-	4.82	5.3.5-5.45	4-7
	2	5.06	6.02	-	-	5.02	5.75	4.5-5.5
Tari [41, 42]	1	4.71	4.21	5.43	-	5.43	-	-
	2	5.12	5.71	5.60	-	5.60	-	-
Some [43]	1	-	-	5.40	-	-	-	-
	2	-	-	5.75	-	-	-	-

characteristics of the dam using data from San Fernando, Alves conducted a forced vibration test in 2002 and developed a finite element model based on it. The results of this test are summarized in Table 3. Another earthquake hit the dam in Chino Hill in 2008. Despite having a magnitude of 5.5, the epicenter was 71 km away from the dam, causing a much lower acceleration of 0.0043g compared to the San Fernando earthquake of 2001, which had an acceleration of 0.164g. The downward acceleration made it possible to assume the dam's linear behavior more confidently. Therefore, this study examines the seismic data of Chino Hills, which is less studied (table 3), after identifying the dynamic characteristics of the dam using the data from San Fernando in 2001[43].

5.1. Identification of the dam system using the seismic data

The main objective of OEM is to minimize the calculation error of predicted results compared to the actual measured data. Previous research has revealed two types of bending modes, symmetric and antisymmetric, in this dam. Therefore, the output data is collected from channels located at the crown level and 80% of the dam height in the radial direction, which includes channels 1, 2, 5, 6, 7, and 8. Additionally, observation channels located in the foundation, including channels 9, 12, and 15, are also considered output. It is important to note that channel 5 data was not recorded properly during the Chino Hills earthquake and, therefore, was not included in system identification. Fig.13 shows the seismic data of channels 5 and 9 in both earthquakes as input and output, respectively. The San Fernando and Chino Hills earthquakes lasted 40 and 60 seconds, respectively, and were sampled at 200 Hz.

It is important to note that the proposed optimization method is sensitive to the starting point. Therefore, to achieve better results, it is recommended to have a stable starting point and always control the extracted models' stability conditions during optimization. According to Verhaegen's recommendation[21], the first sentence's order was 2-3 times the actual order. In this research, the first sentence was considered 8 for both events. Based on the conditions mentioned, the first sentences suitable for both earthquakes are selected, with initial VAF values in Fig.14. After running the algorithm, San Fernando's data converged after 26 attempts and Chino Hills is after 20 attempts, as shown in fig.15. Furthermore, the optimum values of VAF (Fig.14) indicates that the estimation error decreased from 7% to 2% for Chino Hills and 5% to 1% for San Fernando. In the following, the modal specifications that were extracted will be verified.

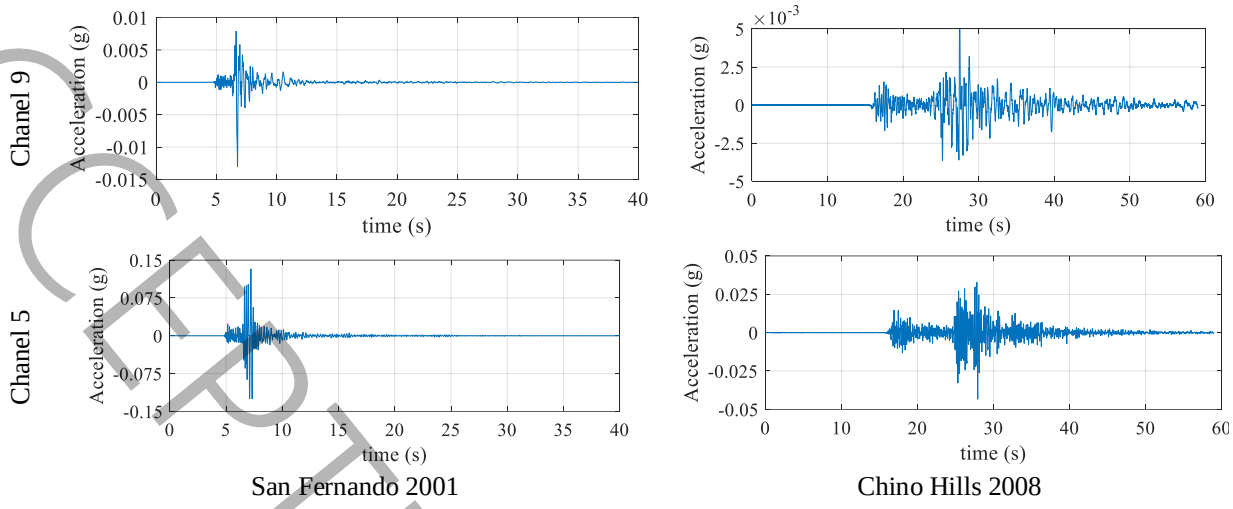

Fig.13. Recorded earthquake responses of observation channels 5 and 9 in the radial direction of Pacoima Dam.

In Fig.16a, the initial modal frequencies for the San Fernando seismic data are 4 and 5 Hz with damping's of 9 and 12, respectively. The convergence of both mode characteristics began at iteration 11 for modal frequencies, with their values remaining constant. The optimization continued until the convergence of the second mode damping at step 15. After the convergence of all four mode characteristics from the 15th iteration, the objective function (Fig.15) and VAF (Fig.14) also reached convergence.

The data optimization process for Chino Hills (as seen in Fig. 15) took longer than the process for San Fernando. As a result, the optimization can be divided into two parts. Before the 10th iteration, the damping ratios did not have appropriate values despite the modal frequencies starting to converge. In the second part, starting from the 11th iteration, the modal frequencies converged to their optimal values, followed by the damping ratios converging to their optimal values. This convergence was accompanied by decreased changes in the objective function (as shown in Fig.15). The final VAF value for Chino Hills data, as shown in Fig. 14, was 98%, 1.5% less than the absolute value for San Fernando data. This difference can be attributed to the unused fifth channel data, as it was in the center of the dam crest. The summary of system identification results for both events can be found in Table 4.

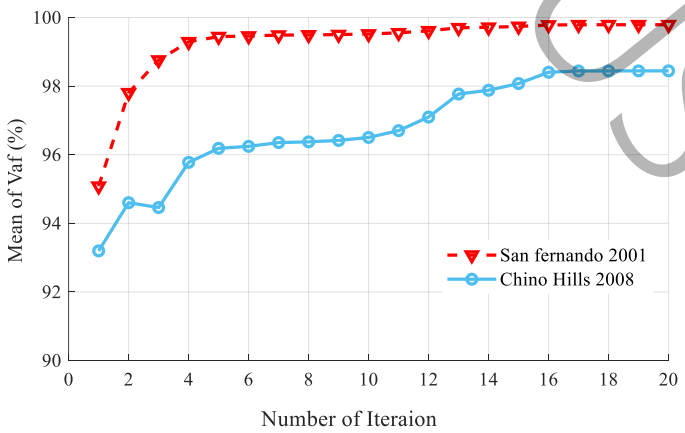

Fig.14. Variance accounting for (VAF) of Pacoima Dam based on San Fernando and Chino Hills seismic monitoring.

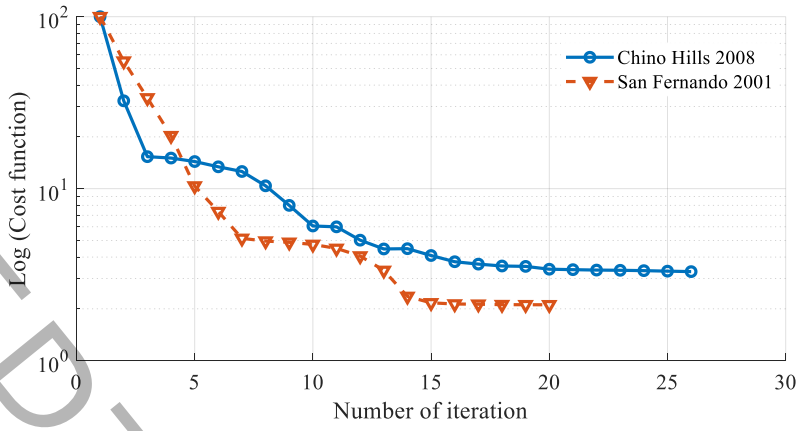

Fig.15. Objective function value evolution process of OEM algorithm based on San Fernando and Chino Hills seismic monitoring.

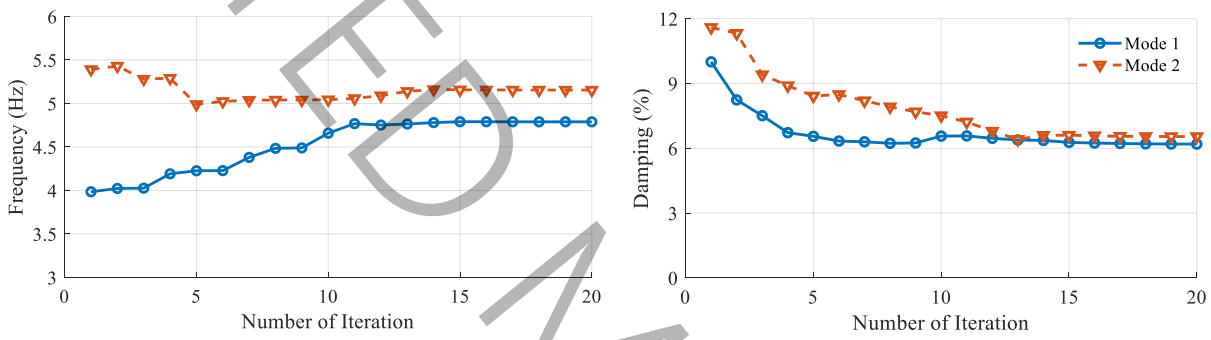

a) Frequency (Hz) b) Daming (%)

Fig.16. System identification process of Pacoima Dam using OEM algorithm based on San Fernando seismic monitoring in 2001.

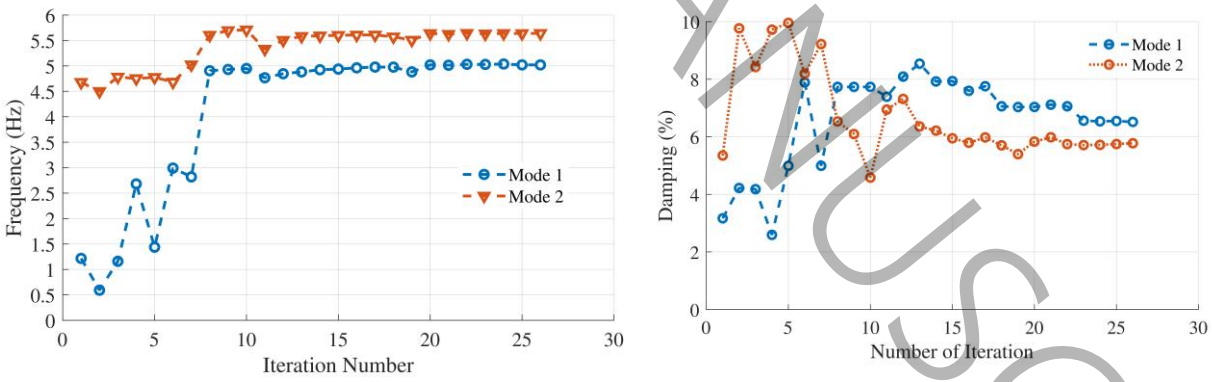

a)San fernando 2001 b) Chino Hills 2008

Fig.17. System identification process of Pacoima Dam using OEM algorithm based on Chino Hills seismic monitoring in 2008.

Table 4. Modal identification results of the identified frequency and damping using OEM algorithm based all seismic monitoring channel data of the dam body, dam foundation of 2001 Fernando and 2008 Chino Hills seismic monitoring.

Mode No.	San Fernando 2001		Chino Hiss 2008	
	Frequency (Hz)	Damping (%)	Frequency (Hz)	Damping (%)
I	4.75	6.35	5.05	6.23
II	5.12	6.05	5.62	5.93

The modal characteristics obtained from the San Fernando data, particularly the modal frequencies, align with the results from previous research. For example, the first mode frequency falls within the 4.73 to 4.83 Hz range, consistent with Alves's findings. The second frequency differs from Alves's results by only 1.17%. The damping ratios obtained in this study are consistent with Alves's findings[39] but differ from Tarinejad's results[44]. This discrepancy may be because subspace methods cannot be utilized to analyze extracted features statistically.

The previous seismic data analysis of Chino Hills showed that the modal frequencies fell within the same range as the forced vibration test results from 2002. This is likely due to the damage caused by previous earthquakes to the dam's structure. Studies suggest that the upper left abutment of the dam is the primary source of the dam's stiffness reduction compared to the dam body. During the Chino Hills earthquake, the structure experienced weak acceleration due to its epicenter from the dam being 71 km away. This resulted in a weak excitation to the foundation system of the dam, which can be compared to the forced vibration test.

The first structural frequency was 5.05 Hz, a 6% decrease compared to the FVT results. The second frequency was also extracted, with a 3% difference from the previous results. This difference and calculation errors are likely due to the decrease in the dam system's stiffness over the past six years. The damping ratio of the first mode falls within the range of the results obtained from the forced vibration test, ranging from 4% to 7%. However, the damping ratio of the second mode is 9% higher than the previous results. To summarize, the proposed method effectively filters the effects of foundation excitation from the seismic data of the dam, and the modal characteristics were extracted with less uncertainty. In the following, the shape modes will be evaluated to determine the reliability of the modal specifications.

The extracted modal shapes from both events are presented in Fig.18. It can be observed that the first and second modes are symmetric and antisymmetric, respectively, which is consistent with the previous findings. Upon analyzing the complexity of the modal shapes (Fig.19), it is observed that the first mode has the minimum MCF in both earthquakes, indicating that the extracted models are highly reliable. The relatively high MCF of the second mode of the Chino- Hills model may be attributed to a calculation error due to the fifth channel's lack of measurement.

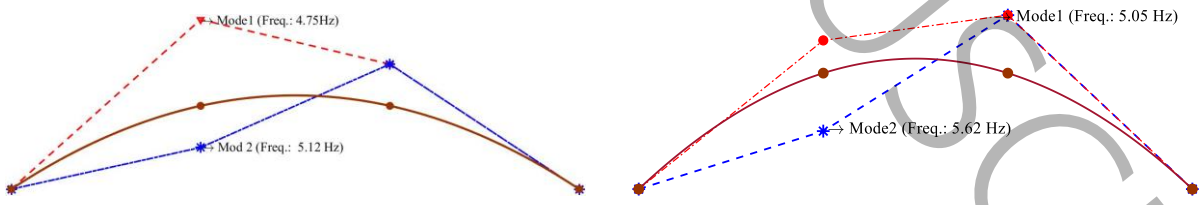

a) San fernando 2001

b) Chino Hills 2008

Fig.18. Shape modes determined using OEM algorithm based on the earthquake responses of San fernando 2001and Chino Hills 2008.

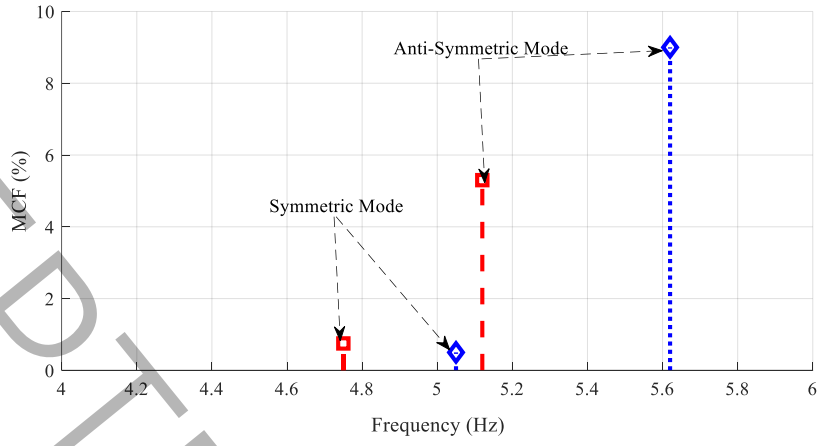

Fig.19. The MCF of identified Mode Shapes using OEM algorithm based all seismic monitoring channel data of the dam body, dam foundation of 2001 Fernando and 2008 Chino Hills seismic monitoring.

6. CONCLUSION

This study emphasizes the challenges associated with using SSI methods. These methods rely heavily on Hankel matrix dimensions and require explicit objective function optimization. The OEM method is suggested for the first time to address these concerns. The process iterates model parameters until the outputs of the simulated model match those of the observed system. The SSI method generates the initial term to reduce the number of optimization steps. However, concurrently, a gradient project minimization must be performed to counteract the state-space consequences of the extracted models' non-injectivity. The method was tested by analyzing a system with a 3-DOF with two closely spaced modes excited by white noise at different noise levels (SNR) of 1, 5, and 15 dB to account for the impact of measurement noise. After analyzing the system, the modal characteristics of the Pacoima Dam were extracted using the 2001 San Fernando and 2008 Chino Hills seismic observations.

The system identification results for the 3-DOF system were almost identical and error-free when predicting low-noise systems with SNR of 5-15dB. However, the damping ratio of the first mode had a more substantial estimated error in the model with SNR=1dB. OEM has worked to reduce the maximum estimation error for the damping ratio from 10% to less than 2%, which has resulted in an improvement in the quality of shape modes by decreasing the complexity of the them by over 75%. The modal characteristics determined from the seismic observations in San Fernando in 2001 were consistent with previous research and the developed finite element model. Additionally, the modal frequencies of Chino Hills from 2008 differed by an average of 4.5% from the results of FVT2002. This difference can be attributed to the decrease in the stiffness of the dam over the past six years of the test, as well as any computational errors.

Overall, when OEM and SSI are combined, the model convergence is quicker, and the estimated models are of higher quality. Moreover, due to the optimization's nature, the suggested approach can be used with minimal settings for automatic or semi-automatic identification in the structure.

References

[1] O.C. Celik, H.P. Gülkan, Processing forced vibration test records of structural systems using the analytic signal, Journal of Vibration and Control, 27(19-20) (2021) 2253-2267.
[2] J.P. Gomes, J.V. Lemos, Characterization of the dynamic behavior of a concrete arch dam by means of forced vibration tests and numerical models, Earthquake Engineering & Structural Dynamics, 49(7) (2020) 679-694.
[3] J. Brownjohn, M. Bocian, D. Hester, Forced vibration testing of footbridges using calibrated human shaker and wireless sensors, Procedia engineering, 199 (2017) 417-422.
[4] M. Viberg, Subspace-based methods for the identification of linear time-invariant systems, Automatica, 31(12) (1995) 1835-1851.
[5] P. Van Overschee, B.L. De Moor, Subspace identification for linear systems: theory, implementation, applications, Kluwer academic publishers Dordrecht, 1996.
[6] V. Verdult, Non linear system identification: a state-space approach, University of Twente, Enschede, The Netherlands, 2002.
[7] K. Peternell, W. Scherrer, M. Deistler, Statistical analysis of novel subspace identification methods, Signal Processing, 52(2) (1996) 161-177.
[8] D. Bauer, M. Deistler, W. Scherrer, User choices in subspace algorithms, in: Proceedings of the 37th IEEE Conference on Decision and Control (Cat. No. 98CH36171), IEEE, 1998, pp. 731-736.
[9] M. Jansson, B. Wahlberg, On consistency of subspace methods for system identification, Automatica, 34(12) (1998) 1507-1519.
[10] P. Van Overschee, B. De Moor, Subspace identification for linear systems: Theory—Implementation—Applications, Springer Science & Business Media, 2012.
[11] P. Van Overschee, B. De Moor, N4SID: Subspace algorithms for the identification of combined deterministic-stochastic systems, Automatica, 30(1) (1994) 75-93.
[12] T. Katayama, Subspace methods for system identification, Springer, 2006.
[13] G. Picci, T. Katayama, Stochastic realization with exogenous inputs and 'subspace-methods' identification, Signal Processing, 52(2) (1996) 145-160.
[14] R.A. Fisher, On the mathematical foundations of theoretical statistics, Philosophical transactions of the Royal Society of London. Series A, containing papers of a mathematical or physical character, 222(594-604) (1922) 309-368.
[15] J.R. Raol, G. Girija, J. Singh, Modelling and parameter estimation of dynamic systems, Iet, 2004.
[16] P. Kabaila, On output-error methods for system identification, IEEE Transactions on Automatic Control, 28(1) (1983) 12-23.
[17] Y. Tomita, A.A. Damen, P.M.V.D. HOF, Equation error versus output error methods, Ergonomics, 35(5-6) (1992) 551-564.
[18] M. Kosaka, H. Uda, E. Bamba, H. Shibata, State-space model identification using input and output data with steady state values zeroing multiple integrals of output error, (2006).
[19] J.J. Moré, The Levenberg-Marquardt algorithm: implementation and theory, in: Numerical analysis, Springer, 1978, pp. 105-116.
[20] B. Peeters, System Identification and Damage Detection in Civil Engeneering, Katholieke Universiteit Leuven, Heverlee (Belgium), 2000.
[21] M. Verhaegen, V. Verdult, Filtering and system identification: a least squares approach, Cambridge university press, 2007.
[22] B. David, Parameter estimation in nonlinear dynamical systems with correlated noise, UCL-Université Catholique de Louvain, 2001.
[23] L.C.S. Góes, E.M. Hemerly, B.C.d.O. Maciel, W.R. Neto, C. Mendonca, J. Hoff, Aircraft parameter estimation using output-error methods, Inverse problems in science and engineering, 14(6) (2006) 651-664.
[24] D.A. Dutra, Collocation-based output-error method for aircraft system identification, in: AIAA Aviation 2019 Forum, 2019, pp. 3087.
[25] M. Brunot, A. Janot, F. Carrillo, J. Cheong, J.-P. Noël, Output error methods for robot identification, Journal of Dynamic Systems, Measurement, and Control, 142(3) (2020) 031002.
[26] S. Dong, T. Liu, W. Wang, J. Bao, Y. Cao, Identification of discrete-time output error model for industrial processes with time delay subject to load disturbance, Journal of Process Control, 50 (2017) 40-55.
[27] C.-T. Chen, Linear system theory and design, Oxford University Press, Inc., United States of America, New York, 1995.

[28] M. Verhaegen, Identification of the deterministic part of MIMO state space models given in innovations form from input-output data, Automatica, 30(1) (1994) 61-74.
[29] J.-H. Weng, C.-H. Loh, J.P. Lynch, K.-C. Lu, P.-Y. Lin, Y. Wang, Output-only modal identification of a cable-stayed bridge using wireless monitoring systems, Engineering Structures, 30(7) (2008) 1820-1830.
[30] M. Verhaegen, Subspace model identification part 3. Analysis of the ordinary output-error state-space model identification algorithm, International Journal of control, 58(3) (1993) 555-586.
[31] M. Verhaegen, P. Dewilde, Subspace model identification part 2. Analysis of the elementary output-error state-space model identification algorithm, International journal of control, 56(5) (1992) 1211-1241.
[32] M. Verhaegen, P. Dewilde, Subspace model identification part 1. The output-error state-space model identification class of algorithms, International journal of control, 56(5) (1992) 1187-1210.
[33] T. McKelvey, A. Helmersson, System identification using an over-parametrized model class-improving the optimization algorithm, in: Proceedings of the 36th IEEE Conference on Decision and Control, IEEE, 1997, pp. 2984-2989.
[34] L.H. Lee, K. Poolla, Identification of linear parameter-varying systems using nonlinear programming, (1999).
[35] M. Pastor, M. Binda, T. Harčarik, Modal assurance criterion, Procedia Engineering, 48 (2012) 543-548.
[36] P. Andersen, Identification of civil engineering structures using vector ARMA models, Aalborg University, Aalborg, Denmark, 1997.
[37] M. Vigsø, T. Kabel, M. Tarpø, R. Brincker, C. Georgakis, Operational modal analysis and fluid-structure interaction, in: Procedings of the International Conference on Noise and Vibration Engineering, ISMA, 2018.
[38] S. Alves, J. Hall, Generation of spatially nonuniform ground motion for nonlinear analysis of a concrete arch dam, Earthquake engineering & structural dynamics, 35(11) (2006) 1339-1357.
[39] S.W. Alves, Nonlinear analysis of Pacoima Dam with spatially nonuniform ground motion, California Institute of Technology, 2005.
[40] S. Alves, J. Hall, System identification of a concrete arch dam and calibration of its finite element model, Earthquake engineering & structural dynamics, 35(11) (2006) 1321-1337.
[41] M. Isari, R. Tarinejad, A. TaghaviGhalesari, A. Sohrabi-Bidar, A new approach to generating non-uniform support excitation at topographic sites, Soils and Foundations, 59(6) (2019) 1933-1945.
[42] R. Tarinejad, Effects of blast loading on the response of concrete arch dam (Case study: Karun 4), Modares Civil Engineering journal, 18(1) (2018) 43-54.
[43] L. Cheng, C. Ma, X. Yuan, J. Yang, L. Hu, D. Zheng, A Literature Review and Result Interpretation of the System Identification of Arch Dams Using Seismic Monitoring Data, Water, 14(20) (2022) 3207.
[44] R. Tarinejad, R. Fatehi, Modal identification of an arch dam during various earthquakes, in: Proceedings of the 1st International Conference On Dams And Hydropower, 2012.